Research Article

Nano Research
2022, 15(7): 6328–6339

ISSN 1998-0124 CN 11-5974/O4
https://doi.org/10.1007/s12274-022-4282-x

STING and TLR7/8 agonists-based nanovaccines for synergistic antitumor immune activation

Bo-Dou Zhang[1], Jun-Jun Wu[1], Wen-Hao Li[1], Hong-Guo Hu[1], Lang Zhao[1], Pei-Yang He[1], Yu-Fen Zhao[1,3], and Yan-Mei Li[1,2] (✉)

[1] *Key Laboratory of Bioorganic Phosphorus Chemistry and Chemical Biology (Ministry of Education), Department of Chemistry, Center for Synthetic and Systems Biology, Tsinghua University, Beijing 100084, China*
[2] *Beijing Institute for Brain Disorders, Beijing 100069, China*
[3] *Institute of Drug Discovery Technology, Ningbo University, Ningbo 315201, China*

Received: 27 December 2021 / **Revised:** 28 February 2022 / **Accepted:** 1 March 2022

ABSTRACT

Immunostimulatory therapies based on pattern recognition receptors (PRRs) have emerged as an effective approach in the fight against cancer, with the ability to recruit tumor-specific lymphocytes in a low-immunogenicity tumor environment. The agonist cyclic dinucleotides (CDNs) of the stimulator of interferon gene (STING) are a group of very promising anticancer molecules that increase tumor immunogenicity by activating innate immunity. However, the tumor immune efficacy of CDNs is limited by several factors, including relatively narrow cytokine production, inefficient delivery to STING, and rapid clearance. In addition, a single adjuvant molecule is unable to elicit a broad cytokine response and thus cannot further amplify the anticancer effect. To address this problem, two or more agonist molecules are often used together to synergistically enhance immune efficacy. In this work, we found that a combination of the STING agonist CDG^{SF} and the Toll-like receptor 7/8 (TLR7/8) agonist 522 produced a broader cytokine response. Subsequently, we developed multicomponent nanovaccines (MCNVs) consisting of a PC7A polymer as a nanocarrier encapsulating the antigen OVA and adjuvant molecules. These MCNVs activate bone marrow-derived dendritic cells (BMDCs) to produce multiple proinflammatory factors that promote antigen cross-presentation to stimulate specific antitumor T-cell responses. In *in vivo* experiments, we observed that MCNVs triggered a strong T-cell response in tumor-infiltrating lymphocytes, resulting in significant tumor regression and, notably, a 100% survival rate in mice through 25 days without other partnering therapies. These data suggest that our nanovaccines have great potential to advance cancer immunotherapy with increased durability and potency.

KEYWORDS

nanovaccines, stimulator of interferon gene (STING), Toll-like receptor 7/8, synergistic immune activation, lymph node targeting

1 Introduction

Cancer immunotherapy, representing a promising method for the treatment of cancer, has been extensively developed in recent years [1–3]. Immunotherapy utilizes the patient's immune system to treat cancer and elicits an effective and durable anticancer immune response. Immune checkpoint blockade (ICB) [4, 5] and cancer vaccination [6–13] are among the methods that have been successful in improving patient survival in the clinic. However, because tumors have multiple mechanisms of immune escape [14], there are few patients who respond positively to immunotherapy. The above issues have stimulated a surge in research to increase the proportion of people who benefit from immunotherapy [15, 16]. Clinical statistics show that patient survival is correlated with tumor specific T cells infiltration into the tumor microenvironment (TME), which become reactivated in response to immunostimulatory molecules [17, 18]. However, many patient tumors lack significant T cell infiltration and are replaced by immunosuppressive cells, which sharply limits antitumor immunity. This has prompted an urgent need to rationally design new strategies to enhance the immune activity of the tumor microenvironment in order to restore antitumor T cell responses.

Pattern recognition receptors (PRRs) are present on innate immune cells, which detect danger-associated molecular patterns. Synergistic activation of PRRs has been explored as a promising cancer therapeutics to generate an amplified immune response [19]. Many recent studies have demonstrated that the cyclic GMP-AMP synthase-stimulator of interferon genes (cGAS-STING) pathway plays an important role in the induction of T cells against cancer [20–23]. The STING pathway can be activated by 2',5-3'5' cyclic guanosine monophosphate–adenosine monophosphate (cGAMP) or cyclic di-GMP (CDG) [24, 25]. Activation of STING triggers type I interferon (IFN-β) and associated proinflammatory cytokines that promote dendritic cell activation and cross-presentation of tumor antigens, subsequently stimulating antitumor T cells [26, 27]. The importance of the STING pathway for the induction of antitumor T cell immune

Address correspondence to liym@mail.tsinghua.edu.cn

responses has revealed cGAMP and structurally related cyclic dinucleotides (CDNs) as promising agents for cancer immunotherapy [28–48]. Despite the great success of STING agonists in preclinical work, recent studies have found that CDN elicits low levels of IL-1β [49, 50], IL-12p70 [51, 52], and IL-6 [53]. However, these three cytokines contribute to the induction of a robust and sustained immune response [53–58]. These cytokines may be produced when Toll-like receptor (TLR) pathways are activated. Therefore, simultaneous activation of the TLR and STING pathways may amplify the antitumor immune response of CDNs. In the present work, we attempted to identify a combination of adjuvant molecules with CDN derivatives that triggers a broader range of cytokines. We subsequently found that the combination of a Toll-like receptor 7/8 (TLR7/8) agonist (522) with STING adjuvant (CDG^{SF}) triggered an immune response that met our expectations. This result is consistent with a previous report that coactivating of TLR7/8 and STING elicit both IL-1β and IL-12p70 [44]. However, the mechanism of the synergistic effect is not known and this synergistic system has not been applied to cancer vaccines. In this work, we studied the mechanism underlying the synergistic effect and applied it to the antitumor vaccine.

Furthermore, although CDNs induce considerable antitumor inflammation [20], their therapeutic efficacy is greatly reduced in the absence of appropriate carriers [45]. Due to the high water solubility and electronegative properties of CDNs, it is difficult for them to cross the cell membrane and activate cytoplasmic STING [45]. Thus, selection of a suitable delivery system is very important to enhance the immunotherapeutic efficacy of CDNs and 522. Adaptive immunity is known to be highly dependent on the efficient trafficking or drainage of antigens to the lymph nodes and the subsequent presentation of processed antigenic information to B and T lymphocytes [59, 60]. Therefore, LNs have served as key targets for delivery of antigens and adjuvants [61, 62]. To further enhance the effect of cancer immunotherapy, we aimed to deliver immune components such as CDNs and 522 to secondary lymphoid tissues. Combining nanotechnology with vaccine therapy can improve the targeting ability of each immune component while reducing its side effects [63]. This offers the possibility to amplify the antitumor immune response. Recently, Gao et al. demonstrated that a cationic polymer (PC7A) with lymph node targeting properties disrupts endosomes and interacts with STING to trigger its activation [47, 64–71]. Hence, the PC7A polymer was chosen as the carrier of the vaccine component.

Here we show that the STING agonist CDG^{SF} [48] synergized with the TLR7/8 agonist 522 [72] to elicit a strong immune response, representing a promising combination of immunostimulants. We subsequently investigated the immune synergistic mechanism between CDG^{SF} and 522, and found that the synergistic effect of STING and TLR7/8 agnoists markedly enhance the function of antigen-presenting cells (APCs) through the NF-κB P65 and TBK-1 signalling pathways. Using a nanoparticle (NP) strategy, the above two adjuvants and tumor antigens were assembled into 50 nm PC7A NPs to obtain multicomponent nanovaccines (MCNVs) (Fig. 1(a)). Through subcutaneous immunization, MCNVs targeted inguinal lymph nodes and enhanced tumor-specific IFN-γ^+ $CD8^+$ T cell responses (Fig. 1(b)), producing excellent therapeutic effects in a mouse model of melanoma. Due to their obvious tumor suppressive effects, the MCNV system represents a general platform for tumor immunotherapy.

2 Experimental

2.1 Materials

CDG^{SF} [48], PC7A polymer nanoparticles [64], and 522 [73] were

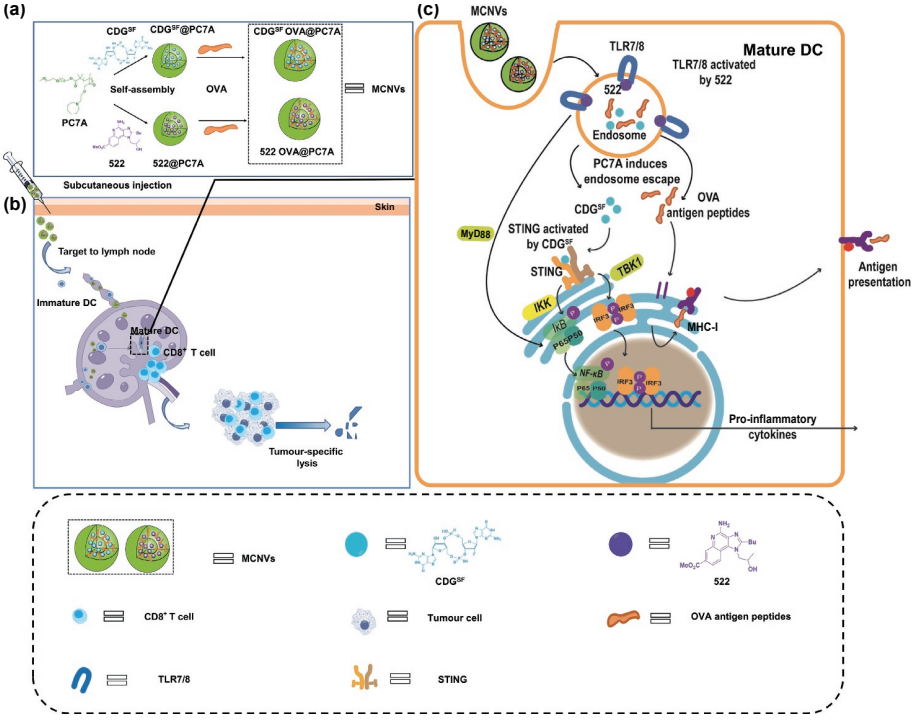

Figure 1 Fabrication and antitumor immune responses of MCNVs. (a) MCNVs were prepared following a solvent evaporation method [65, 66]. (b) Schematic depiction of MCNVs carrying adjuvants and OVA epitopes into lymph nodes, effectively modulating adaptive and innate immune responses for cancer immunotherapy. (c) Mechanism of immune synergy between CDG^{SF} and 522. When MCNVs are taken up by APCs, they disassemble within the endosomal compartment in response to low pH conditions, causing subsequent release of 522, CDG^{SF}, and OVA. Then, 522 activates TLR7/8 on the endosomal membrane and CDG^{SF} stimulates STING in the cytoplasm, promoting APC maturation and antigen presentation. We further demonstrate that 522 and CDG^{SF} synergistically enhance the function of APCs through the NF-κB P65 and TBK-1 signalling pathways.

synthesized according to the reported literature. All compounds were consistent with the data reported in the literature. 2-Aminomalononitrile 4-methylbenzenesulfonate, 2-amino-4-(methoxycarbonyl)benzeneboronic acid hydrochloride, CH_2I_2, PPh3, and trimethyl orthovalerate were purchased from Meryer (Shanghai, China). $Pd(OAc)_2$ and NEt_3 were purchased from Adamas. DL-1-amino-2-propanol was purchased from Acros. Methacryloyl chloride, N,N,N',N'',N''-Pentamethyldiethylenetriamine, 1H-azepine-1-ethanol, and copper(I) bromide were purchased from Innochem. All amino acids and resins were purchased from GL Biochem (Shanghai, China) Ltd. Fetal bovine serum (FBS) was purchased from Gibco Life Technologies. CpG oligonucleotide and polyinosinic-polycytidylic acid (poly(I:C) (low molecular weight) was purchased from Invivogen. Penicillin-streptomycin and fluorescein5(6)-isothiocyanate were purchased from Sigma-Aldrich. RPMI-1640 and phosphate-buffered saline (PBS, pH 7.4) were purchased from Corning. All chemicals used in the experiments were obtained from commercial sources and used without further purification. All solvents were of reagent/high-performance liquid chromatography (HPLC) grade.

2.2 Enzyme-linked immunosorbent assay (ELISAs) kits

IL-1β, IL-12p70, IL-6, TNF-α, CXCL10, IFN-γ, and IFN-β were purchased from DAKEWA. MyD88, NF-κB P65, and TBK-1 were purchased from ELISA Genie.

2.3 Synthesis of CDG^{SF}, 522, PC7A, and antigen peptides

The detailed synthetic procedures were descripted in the Electronic Supplementary Material (ESM).

2.4 Preparation and characterization of MCNVs

The detailed procedures were descripted in the ESM.

2.5 Cells and animals experiments

Bone marrow-derived dendritic cells (BMDCs) and B16-OVA cell line were cultured in RPMI-1640 (10% heat-inactivated FBS, 100 μg/mL streptomycin and 100 U/mL penicillin). Preparation of BMDCs, bone marrow were removed from female C57BL/6 mice (6 weeks), treated with erythrocyte lysate and cultured with RPMI 1640 complete medium (10% heat-inactivated FBS, 100 μg/mL streptomycin, 100 U/mL penicillin, and 20 ng/mL GM-CSF). The medium was replenished on day 3, half the volume of the old medium was replaced with fresh medium on day 6, and BMDCs were harvested on day 9. All animal experiments were performed according to the institutional guidelines for animal welfare and were approval by the Institutional Animal Care and Use Committee (IACUC) at Tsinghua University. The laboratory animal facility has been accredited by Association for Assessment and Accreditation of Laboratory Animal Care International (AAALAC). Female C57BL/6 mice were obtained and housed in a facility of the Center of Biomedical Analysis at Tsinghua University.

2.6 *In vitro* evaluation of MCNVs activity

For *in vitro* screening of CDG^{SF} with pathogen-associated molecular pattern (PAMPs), BMDCs were treated with PBS, CDG^{SF} (1 μg/mL), 522 (1 μg/mL), poly(I:C) (10 μg/mL), CpG (1 μg/mL), CDG^{SF} (0.5 μg/mL) + poly(I:C) (5 μg/mL), CDG^{SF} (0.5 μg/mL) + CpG (0.5 μg/mL), CDG^{SF} (0.5 μg/mL) + 522 (0.5 μg/mL), CDG^{SF}@PC7A (13.1 μg/mL), 522@PC7A (16.4 μg/mL), and CDG^{SF}@PC7A (13.1 μg/mL) + 522@PC7A (16.4 μg/mL), respectively. The cell supernatants were collected after 24 h of incubation and analyzed for IL-1β, IL-12p70, IL-6, TNF-α, CXCL10, IFN-β, MyD88, NF-κB P65, and TBK-1 ELISA kits.

We assessed whether the introduction of the polymer affected the immunostimulatory function of CDG^{SF} and 522. BMDCs were incubated for 24 h with PBS, OVA, OVA@PC7A, CDG^{SF} + 522 + OVA, CDG^{SF} OVA@PC7A, 522 OVA@PC7A, and MCNVs. (OVA: 1 μg/mL, CDG^{SF}: 0.5 μg/mL, 522: 0.5 μg/mL). The cells and cell supernatants were collected after 24 h of incubation and analyzed by flow cytometry or with IL-1β, IL-12p70, IL-6, TNF-α, CXCL10, and IFN-β ELISA kits. The surface markers of BMDCs were then stained with fluorophore-labeled antibodies (BioLegend) (PB-conjugated anti-CD11c, PE-conjugated anti-CD86, APC-conjugated anti-CD80, and PE/CY7-conjugated anti-H-$2K^b$/SIINFEKL antibodies).

2.7 *In vivo* fluorescence imaging

We next investigated whether MCNVs could target lymph nodes. Female C57BL/6 mice (6–8 weeks) were subcutaneously injected with various formulations at the tail base, including FAM-OVA (50 μg per mouse), CDG^{SF} (3.5 μg per mouse) + 522 (3.5 μg per mouse), and CDG^{SF}@PC7A (91 μg per mouse) + 522@PC7A (114.6 μg per mouse) in 100 μL injection volume. The migration of MCNVs was imaged *in vivo* for 3 days (72 h) using an *in vivo* imaging system (IVIS) spectrum imaging system (PerkinElmer).

2.8 *In vivo* immune activation

To determine the activation of the LNs, mice were subcutaneously immunized with various antigen-containing formulations, including OVA-FAM (10 nmol per mouse), CDG^{SF} (3.5 μg per mouse) + 522 (3.5 μg per mouse), and CDG^{SF}@PC7A (91 μg per mouse) + 522@PC7A (114.6 μg per mouse) in 100 μL injection volume. The inguinal LNs were collected at 24 h injection, and lymphocytes were used for flow cytometry analysis (Fig. S8 in the ESM). The surface markers of lymphocytes were then stained with fluorophore-labeled antibodies (BioLegend) (PB-conjugated anti-CD11c, PE-conjugated anti-CD86, and APC-conjugated anti-H-$2K^b$/SIINFEKL antibodies).

C57BL/6J mice were subcutaneously immunized with formulations as described. Seven days after the last immunization, 6×10^6 spleen cells per well were added into 24-well plates and retreated with 50 μg/mL OVA for 96 h. The IFN-γ in the cell supernatants was assessed by using IFN-γ ELISA kits (DAKEWA). Splenocytes were collected for flow cytometry analysis (Fig. S8 in the ESM) (APC-conjugated anti-CD3 (BioLegend), FITC-conjugated anti-CD8 (BioLegend), and PE-H-2 kb/SIINFEKL tetramer (MBL) staining of $CD8^+$ T cells in the spleen).

2.9 *In vivo* antitumor activity

To further investigate the antitumor effects of MCNVs, B16-OVA tumor cells (1.5×10^5, expressing the OVA epitope on the B16 tumor) were subcutaneously injected into the right side of 4 to 6-week-old C57BL/6 mice (n = 7). On day 10 posttransplantation, the tumors reached 5 mm in diameter and the vaccines (OVA (10 nmol per mouse), CDG^{SF} (3.5 μg per mouse) + 522 (3.5 μg per mouse), and CDG^{SF}@PC7A (91 μg per mouse) + 522@PC7A (114.6 μg per mouse) in 100 μL injection volume) were subcutaneously injected into the peritumor area (Fig. 7(a)). Survival rate and tumor growth were monitored every other day in all groups. Tumor volume: 0.5 × length × $width^2$. Mice were euthanized when the tumors reached 1.5 cm in length. Splenocytes were prepared as described above. Tumor tissues were collected and ground into single-cell suspensions for flow cytometric analysis (Fig. S8 in the ESM). Tumor-infiltrating T cells (TILs), splenocytes, and natural killer (NK) cells were stained with several panels of antibodies (BioLegend): PerCP-Cy5.5-conjugated

anti-CD45, APC-conjugated anti-CD3, PB-conjugated anti-CD4, FITC-conjugated anti-CD8, APC/CY7-conjugated anti-NK1.1, and PE-conjugated anti-CD69. For IFN-γ analysis, TILs and splenocytes were cultured in 24-well plates and stimulated with OVA/ionomycin/brefeldin (BioLegend) for 4 h. The cells were then stained with APC-conjugated anti-CD3, PB-conjugated anti-CD4, and FITC-conjugated anti-CD8 antibodies. After fixation and permeabilization, the cells were further strained with PE-conjugated anti-IFN-γ (BioLegend). To analyze the memory cells of the spleen, splenocytes were stained with several panels of antibodies (BioLegend): APC-conjugated anti-CD3, PB-conjugated anti-CD4, FITC-conjugated anti-CD8, PE-conjugated anti-CD44, and PE/CY7-conjugated anti-CD62L.

3 Results and discussion

3.1 CDG^{SF} combined with 522 elicited a broader cytokine response

Recently, a growing number of studies have demonstrated the critical importance of activating STING and stimulating the generation of type I IFN production in the antitumor immune response [20–23]. However, despite this success, recent work has found that activation of the STING pathway alone only produces a relatively narrow range of cytokines and does not include some of the cytokines that contribute to a robust and long-term antitumor response, most notably IL-1β [49, 50], IL-12p70 [51, 52], and IL-6 [53], which play important roles in the generation of adaptive immune responses [74, 75]. Therefore, in this work, we proposed identifying complementary strategies to facilitate more powerful activation of the STING pathway for antitumor immunity. We aimed to identify PAMP adjuvants capable of generating a complementary cytokine pool containing IL-1β, IL-12p70, and IL-6. Among all PRRs, those related to nucleic acid recognition (TLR3, TLR7/8, and TLR9) are located in intracellular compartments, some of which have demonstrated synergistic effects [76–79]. Therefore, we tested the STING pathway adjuvant combination using several intracellular adjuvant molecules (TLR3 agonist poly(I:C) [80], TLR7/8 agonist 522 [72], and TLR9 agonist CpG [81]). In follow-up work, we used the STING adjuvant (thiophosphate and fluorine modification cyclic di-GMP derivatives (CDG^{SF})) we recently reported [48], which possesses higher stability and immune reactivity in mice. BMDCs were incubated with CDG^{SF} alone or combined with different adjuvant molecules.

Notably, to diminish dose-related activation effects, both agonists were halved in the combination groups. Among the groups of adjuvants examined, CDG^{SF} + 522 induced the high levels of IL-1β, IL-12p70, and IL-6, which were not achieved by CDG^{SF} alone or in combination with poly(I:C) and CpG (Figs. 2(a) and 2(b)). Similarly, the CDG^{SF} + 522 combination enhanced the production of TNF-α compared to CDG^{SF} alone (Figs. 2(c) and

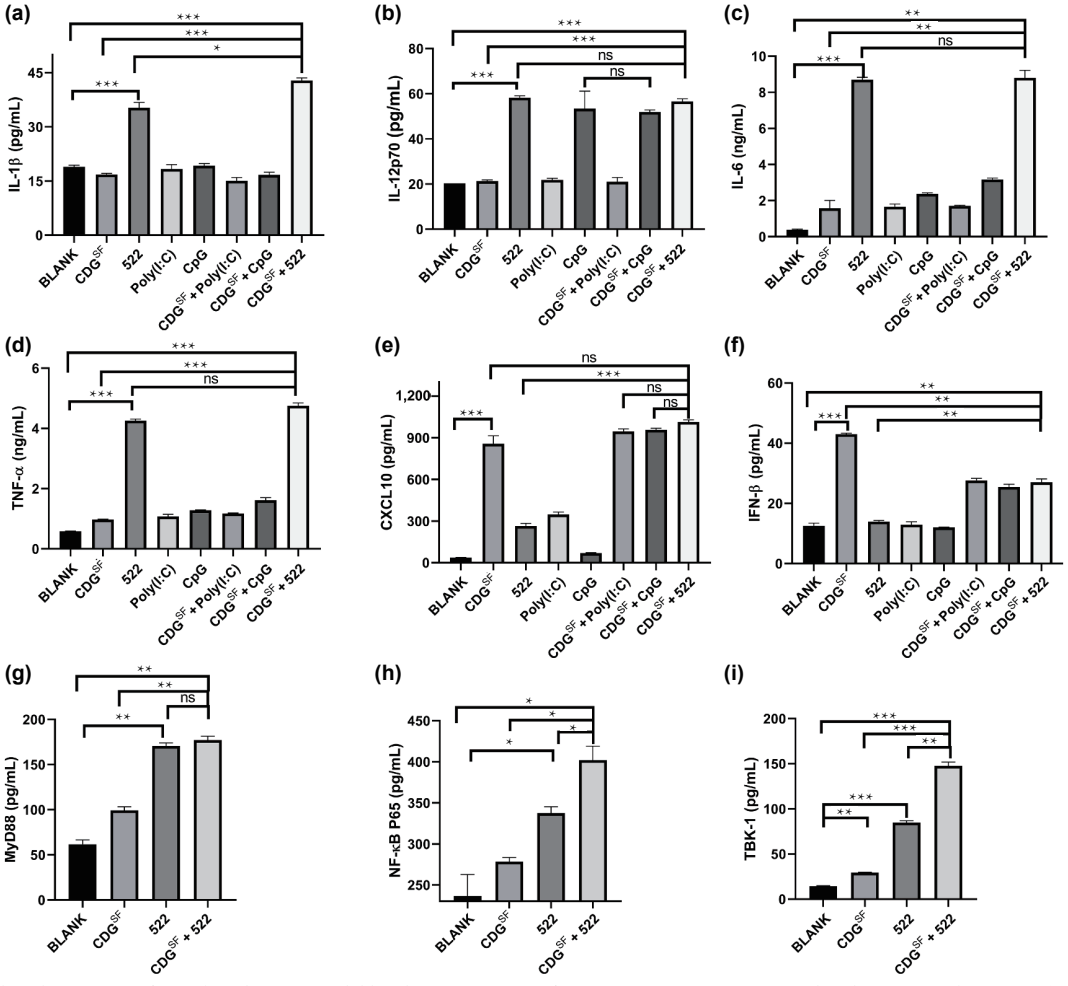

Figure 2 Combined treatment of CDG^{SF} with various soluble adjuvants. BMDCs from C57BL/6 mice were treated with PBS, CDG^{SF} (1 μg/mL), 522 (1 μg/mL), poly(I:C) (10 μg/mL), CpG (1 μg/mL), CDG^{SF} (0.5 μg/mL) + poly(I:C) (5 μg/mL), CDG^{SF} (0.5 μg/mL) + CpG (0.5 μg/mL), and CDG^{SF} (0.5 μg/mL) + 522 (0.5 μg/mL), respectively. The cells and cell supernatants were collected after 24 h of incubation and analyzed for (a) IL-1β, (b) IL-12p70, (c) IL-6, (d) TNF-α, (e) CXCL10, (f) IFN-β, (g) MyD88, (h) NF-κB P65, and (i) TBK-1. The results are shown as the mean ± SD of three independent experiments; ns: no significant difference, $^{*}p < 0.05$, $^{**}p < 0.01$, and $^{***}p < 0.001$ by one-way analysis of variance (ANOVA) with Tukey's test.

2(d)). However, the dose of CDG^{SF} in the combination was half that of CDG^{SF} alone, and there was some reduction in proinflammatory CXCL10 and IFN-β cytokine release from BMDCs after stimulation with CDG^{SF} + 522 (Figs. 2(e) and 2(f)).

The above results indicate that CDG^{SF} + 522 effectively improves the limitations of CDG^{SF}. This combination was therefore chosen for further immunostimulatory mechanistic study. An increase in expression of the costimulatory molecule CD86 is an essential condition for complete activation of T cells and induces antitumor T cell activity. After incubating each group with BMDC for 24 hours, the CDG^{SF}+522 group showed a higher level of CD86 expression compared to the CDG^{SF} group, but was not significantly different from the 522 group (Fig. S1 in the ESM). To further investigate the pathways involved in cytokine secretion, the levels of MyD88, NF-κB P65, and TBK-1 in BMDCs stimulated with CDG^{SF} and/or 522 for 24 h were measured by ELISA kits. In the control groups, levels of MyD88, NF-κB P65, and TBK-1 remained at baseline. The CDG^{SF} + 522 group stimulated BMDCs to express higher MyD88 than the control group, but was not significantly different from the 522 alone group (P65, and TBK-1 remained at baseline. The CDG^{SF} + 522 group stimulated BMDCs to express higher MyD88 than the control group, but was not significantly different from the 522 alone group (Fig. 2(g)). In contrast, levels of NF-κB P65 and TBK-1 were highest in CDG^{SF} + 522 group (Figs. 2(h) and 2(i)). These results demonstrate that the synergy of STING and TLR7/8 ligands may enhance the function of DCs through the NF-κB P65 and TBK-1 signalling pathways, confirming that CDG^{SF} + 522 is a promising combination of immunostimulants.

3.2 Preparation and characterization of MCNVs

Based on the above results, the two adjuvant molecules CDG^{SF} and 522 were chosen for subsequent immune study in this work. However, CDN derivatives are negatively charged and highly water-soluble, making it challenging for them to cross the cell membrane to activate the STING pathway [45]. Furthermore, systemic administration of immunostimulants disrupts immune homeostasis at nontarget sites [82]. In contrast, nanodelivery techniques effectively accumulate adjuvant molecules on specific tissues or cells [63, 83], reducing the toxic effects of adjuvants. Secondary lymphoid tissue near the tumor contains a large number of lymphoid T and B cells [59, 60], representing a promising nanodelivery strategy to enrich immunostimulants and tumor antigens in lymph nodes and subsequently stimulate lymphocytes to eradicate cancer cells [61, 62]. Notably, Gao et al. synthesized ultrapH-sensitive nanoparticles (PC7A NPs), that can not only target lymph nodes, but also directly activate the STING pathway [65]. In addition, PC7A NPs release immune components by disassembling in the endosome under low pH conditions [47, 66]. Due to these above advantages, we chose PC7A NPs as the carrier for our immunostimulants cocktail. Herein, adjuvant molecules and PC7A are assembled under sonication conditions to form NPs. The NPs were then mixed with the OVA peptide for 30 min at room temperature, free OVA was removed by ultrafiltration, and then MCNVs (CDG^{SF} OVA@PC7A + 522 OVA@PC7A) were obtained (Fig. 1(a)).

MCNVs were approximately 80 nm at pH 7.4, as measured by transmission electron microscopy, while NP dissolution was observed at pH 4.7. This demonstrates that the PC7A polymer has nanosized and pH-responsive capability (Fig. 3(a)). The adjuvants and antigen encapsulation efficiency (EE%) were measured by ultrafiltration method (Table S1 in the ESM). The internalization of MCNVs in BMDCs was next investigated using flow cytometry. MCNVs were labelled with OVA-carboxyfluorescein (MCNVs-FAM) and incubated with BMDCs for 8 h. The results showed that MCNVs increased the uptake of OVA-FAM by BMDCs compared to the control and groups (Fig. 3(b)).

We next determined the ratio of CDG^{SF}@PC7A and 522@PC7A that produced optimal immunostimulatory activity. BMDCs were treated with the indicated ratios of CDG^{SF}@PC7A and 522@PC7A for 24 h, and BMDCs were subsequently tested by flow cytometric analysis. We analyzed the surface expression of costimulatory molecules and maturation receptors (CD86, CD80, and CCR7). The data for CD86, CD80, and CCR7 showed that the optimal immunostimulatory response occurred at a 1:1 weight ratio of CDG^{SF}@PC7A to 522@PC7A (Figs. S2(a)–S2(c) in the ESM). Therefore, we used this ratio for subsequent experiments.

3.3 MCNVs enhances immunostimulatory functions in BMDCs

We next assessed whether the introduction of the polymer affected the immunostimulatory function of CDG^{SF} and 522. BMDCs were incubated with each group (OVA, OVA@PC7A, CDG^{SF} + 522 + OVA, CDG^{SF} OVA-FAM@PC7A, 522 OVA@PC7A, and MCNVs). Inflammatory cytokine experiments demonstrated that MCNVs stimulation of BMDCs induced higher levels of IL-1β, IL-

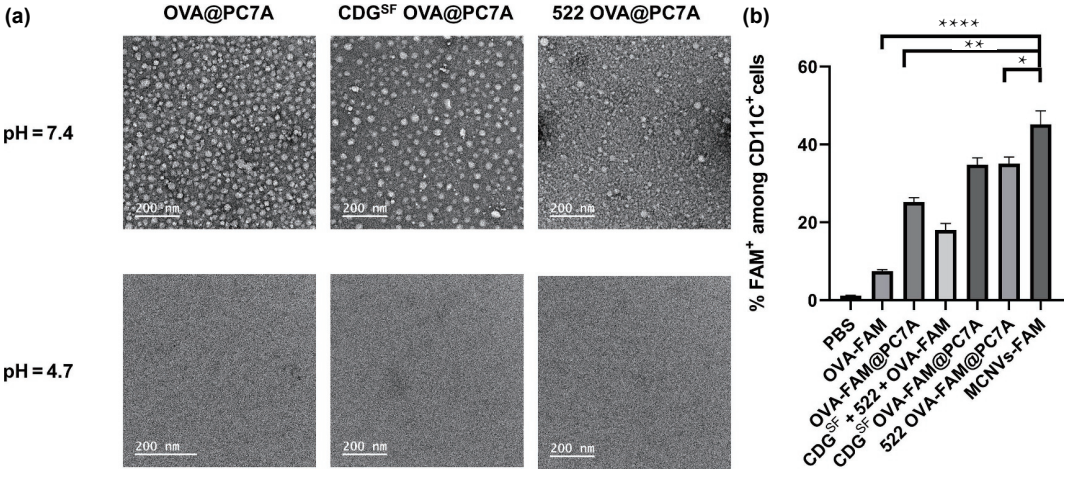

Figure 3 Characterization of MCNVs. (a) Transmission electron microscopy image of NPs in pH 7.4 and pH 4.7 buffers. (b) Internalization of MCNVs (FAM-OVA) in BMDCs was detected by flow cytometry. BMDCs were treated with 1.2 μg OVA-FAM per well (OVA-FAM, OVA-FAM@PC7A, CDG^{SF} + 522 + OVA-FAM, CDG^{SF} OVA-FAM@PC7A, 522 OVA-FAM@PC7A, and MCNVs-FAM). BMDCs were collected after 8 h of incubation and analyzed by flow cytometry (%FAM^+/$CD11c^+$). Data are representative of three independent experiments, ns: no significant difference, *$p < 0.05$, **$p < 0.01$, and ***$p < 0.001$ by one-way ANOVA with Tukey's test.

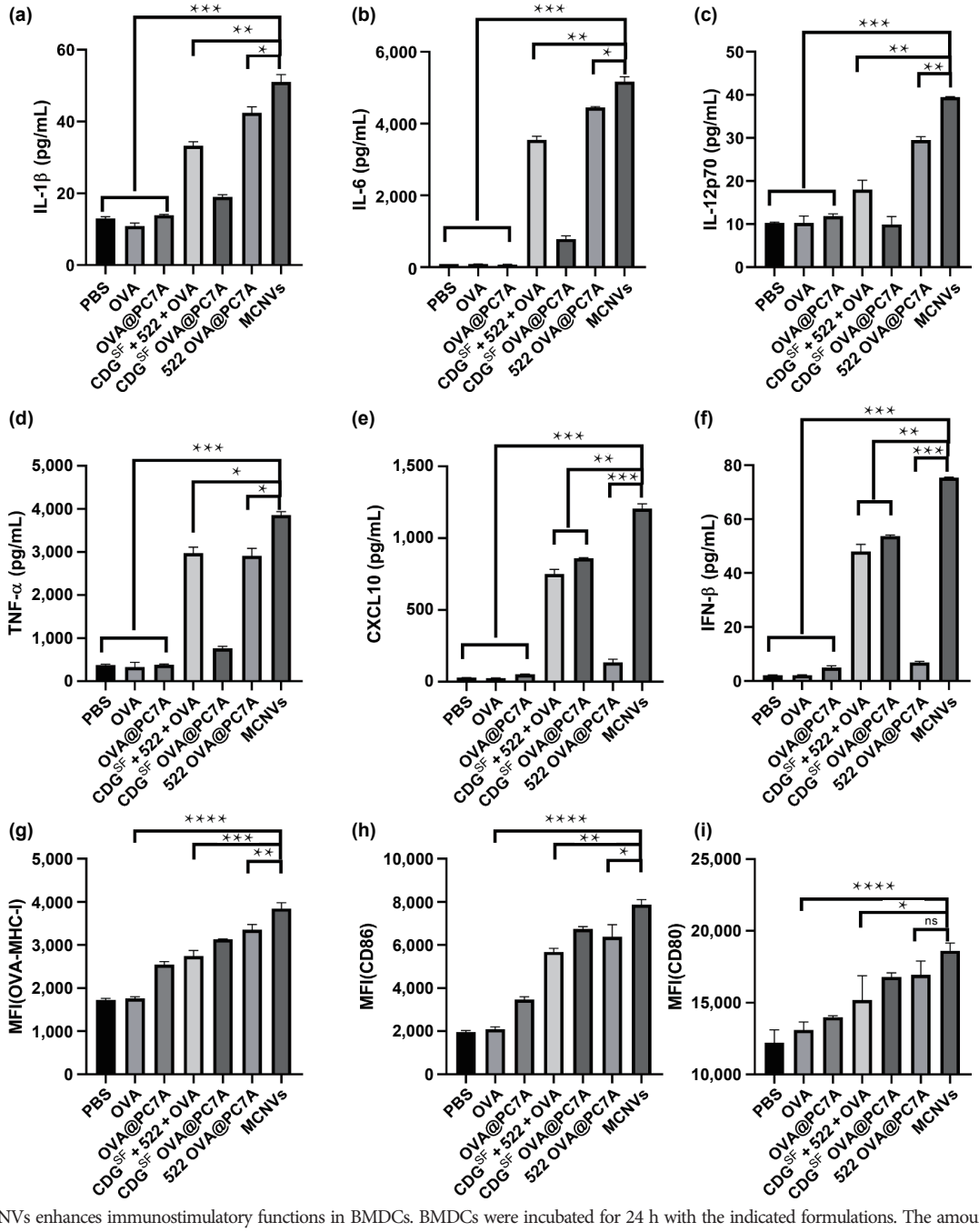

Figure 4 MCNVs enhances immunostimulatory functions in BMDCs. BMDCs were incubated for 24 h with the indicated formulations. The amount of CDG^{SF} or 522 in each group was 0.5 μg/mL. Cytokines released ((a) IL-1β, (b) IL-6, (c) IL-12p70 , (d) TNF-α, (e) CXCL10, and (f) IFN-β) in BMDCs. Relative expression levels of maturation markers ((g) OVA-MHC-I, (h) CD86, and (i) CD80) expressed as the mean fluorescence intensity of each marker in BMDCs (CD11c + cells). Data are representative of three independent experiments, ns: no significant difference, $^{*}p < 0.05$, $^{**}p < 0.01$, and $^{***}p < 0.001$ by one-way ANOVA with Tukey's test.

6, IL-12p70, TNF-α, CXCL10, and IFN-β than the free adjuvants and single adjuvant nanoparticles (Figs. 4(a)–4(f)). We previously demonstrated that PC7A carriers contribute to the accumulation of OVA antigens in cells, and further investigated the process of antigen cross-presentation (Figs. 4(g)–4(i)). After 24 h of incubation, we analyzed the cell surface expression of antigen loaded major histocompatibility complex class I (OVA-MHC-I) by flow cytometry. As shown in Fig. 4(g), MCNV treatment upregulated OVA-MHC-I compared to CDG^{SF} + 522 + OVA, indicating that the MCNV system significantly enhanced antigen expression. In addition, MCNVs-treated cells also upregulated OVA-MHC-I compared to CDG^{SF} OVA@PC7A and 522 OVA@PC7A, which further validated the synergistic effect of CDG^{SF} and 522. Next, to investigate whether MCNVs also affect BMDC maturation, we analyzed the surface expression of costimulatory molecules (CD86 and CD80). High expression of costimulatory molecules CD80 and CD86 is required to activate T cell maturation. The results showed that BMDCs treated with MCNVs exhibited high expression levels of CD86 and CD80 (Figs. 4(h) and 4(i)). These data suggest that MCNVs elicited higher immune activation than CDG^{SF} + 522 + OVA, possibly due to the increased intracellular delivery efficiency of adjuvant molecules by PC7A.

3.4 *In vivo* trafficking of MCNVs to the lymph nodes

LNs are a critical bridge between innate and adaptive immunity where activated APCs can interact with B and T cells [59, 60]. Therefore, efficient delivery of immunostimulatory components to LNs elicits a strong immune response [61, 62]. Due to its optimal size (70 nm), MCNVs may reach the lymph nodes through the lymphatic vessels, and we next investigated whether MCNVs could target lymph nodes. C57BL/6 mice were subcutaneously

injected with OVA-FAM labelled MCNVs, and the migration of MCNVs was imaged *in vivo* for 3 days (72 h) using a IVIS spectrum imaging system (PerkinElmer). At 24 h postinjection, fluorescence signals of proximal LNs were detected in all groups except the control group, while the strongest signals were observed for MCNVs-FAM. Subsequently, the fluorescence signal of distal LNs in the nanocarrier groups gradually increased from 24 to 48 h after injection, and the strongest fluorescence signal was observed in the MCNVs group. Seventy-two hours after injection, the fluorescence signal of the proximal lymph nodes in the control group gradually decreased, while the intensity of the fluorescence signal in the MCNVs group was basically unchanged (Fig. 5(a)). These data suggest that MCNVs system not only increased the accumulation of FAM-OVA proximal LNs, but also facilitated the migration of FAM-OVA from the injection site to distal LNs. We then analyzed lymphocytes in LNs 24 h after injection. Mice treated with MCNVs exhibited the largest proportion of FAM-OVA uptake and the highest expression levels of OVA-MHC-I and CD86, consistent with the results of *in vitro* stimulation experiments (Fig. 5(b)). In conclusion, MCNVs both prolong and increase the accumulation of antigens in LNs, thereby increasing the probability of eliciting an effective antitumor immune response.

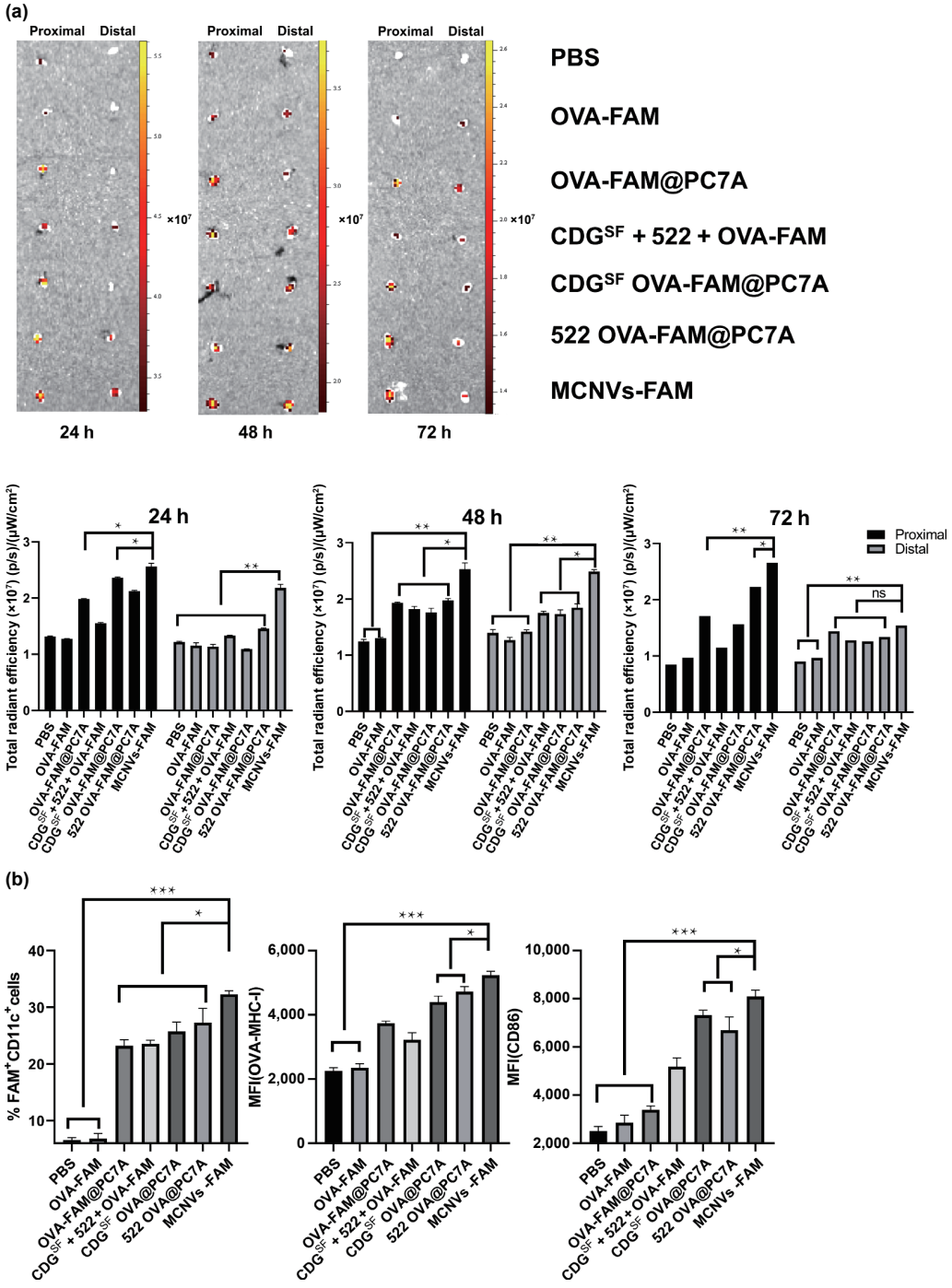

Figure 5 *In vivo* trafficking of MCNVs to the lymph nodes. C57BL/6J mice were s.c. injected with the indicated formulations (1. PBS, 2. OVA-FAM, 3. OVA-FAM@PC7A, 4. CDG^{SF} + 522 + OVA-FAM, 5. CDG^{SF} OVA-FAM@PC7A, 6. 522 OVA-FAM@PC7A, 7. MCNVs-FAM), and the dose of OVA-FAM was 50 μg per mouse, respectively. (a) After 24 h (left), 48 h (mid), and 72 h (right), the LNs were analyzed using a IVIS spectrum imaging system (PerkinElmer), and the corresponding fluorescent quantitation is shown (n = 3). (b) The percentage of FAM$^+$CD11c$^+$ DCs, and relative expression levels of maturation markers (OVA-MHC-I and CD86) expressed as the mean fluorescence intensity of each marker in DCs are shown (n = 3). The results are shown as the mean ± SD of three independent experiments. ns: no significant difference, $^*p < 0.05$, $^{**}p < 0.01$, and $^{***}p < 0.001$ by one-way ANOVA with Tukey's test.

3.5 *In vivo* immune activity of MCNVs

To further investigate the *in vivo* immunization effect of MNCVs, C57BL/6 mice were subcutaneously immunized with different groups of vaccines (PBS, OVA, OVA@PC7A, CDG^{SF} + 522 + OVA, CDG^{SF} OVA@PC7A, 522 OVA@PC7A, and MCNVs) every 4 days a total of three times (Fig. 6(a)). Seven days after the last immunization, the spleens of the mice were collected and analyzed for activation levels of immune cells. Th1 cytokines (e.g., IFN-γ) not only directly promote specific antibody production, but also mediate cytotoxic T lymphocyte (CTL) responses. MCNV-immunized mouse spleen lymphocytes exhibited increased OVA-specific IFN-γ production compared to free CDG^{SF} + 522 + OVA and single adjuvant nanoparticles (Fig. 6(b)). This result was confirmed by $CD8^+$ T cell triggering assays, where OVA (SIINFEKL)-specific $CD8^+$ T cells exhibited higher proliferation in MCNVs than in the other groups (Fig. 6(c)). This result demonstrates that MCNVs stimulate the immune system to produce tumor-specific $CD8^+$ T cells.

3.6 MCNVs enhance vaccine efficacy against aggressive B16-F10 (OVA) melanoma cells

To further investigate the antitumor effects of MCNVs, B16-OVA tumor cells (1.5×10^5, expressing the OVA epitope on the B16 tumor) were subcutaneously injected into the right side of 4 to 6-week-old C57BL/6 mice (n = 7). On day 10 posttransplantation, the tumors reached 5 mm in diameter and the vaccines were injected into the subcutaneous area around the tumor. As illustrated in (Figs. 7(b) and 7(c)), all animals in the PBS control group died within 21 days. OVA alone did not provide any significant tumor growth inhibition or survival benefit compared to the PBS control. The OVA@PC7A, CDG^{SF} + 522 + OVA, CDG^{SF} OVA@PC7A, and 522 OVA@PC7A groups had relatively low antitumor effects. In contrast, the MCNV-treated mice displayed the smallest tumor volumes, and 100% of them survived longer than 25 days.

To explore antitumor effects of MCNVs, lymphocytes from spleen and tumor tissues were extracted for analysis. CD69, a marker of early T cell activation was expressed by splenic T cells, and mice treated with MCNVs expressed higher levels of $CD8^+CD69^+$ than the free adjuvant and single adjuvant nanoparticle groups (Fig. 7(d)). We further found that mice immunized with MCNVs displayed a significantly increased proportion of $CD44^+CD62L^-CD8^+$ effector memory T (Tem) cells and $CD44^+CD62L^+CD8^+$ central memory T (Tcm) cells in the spleen (Fig. 7(e)). This indicates the acquisition of memory T-cell immunity for immune surveillance. Next, we evaluated the effect

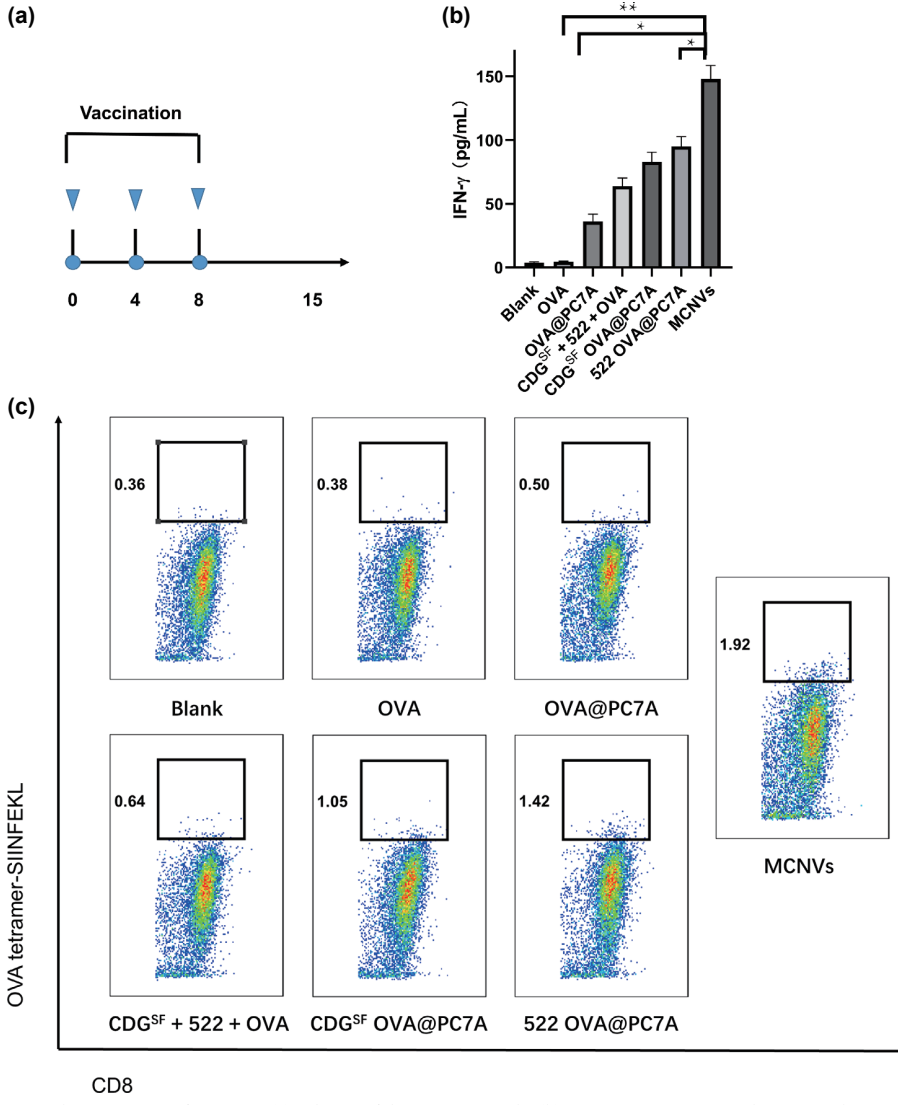

Figure 6 *In vivo* immunostimulatory activity of MCNVs. (a) Scheme of the immune study. (b) C57BL/6J mice were subcutaneously immunized with formulations as described. Seven days after the last immunization, 6×10^6 spleen cells per well were added into 24-well plates and retreated with 50 μg/mL OVA for 96 h. The IFN-γ in the cell supernatants was assessed by using ELISA kits. (c) Representative flow dot plots of H-2kb/SIINFEKL tetramer staining of $CD8^+$ T cells in the spleen. The results are shown as the mean ± SD of three separate experiments. ns: no significant difference, $^*p < 0.05$, $^{**}p < 0.01$, and $^{***}p < 0.001$ by one-way ANOVA with Tukey's test.

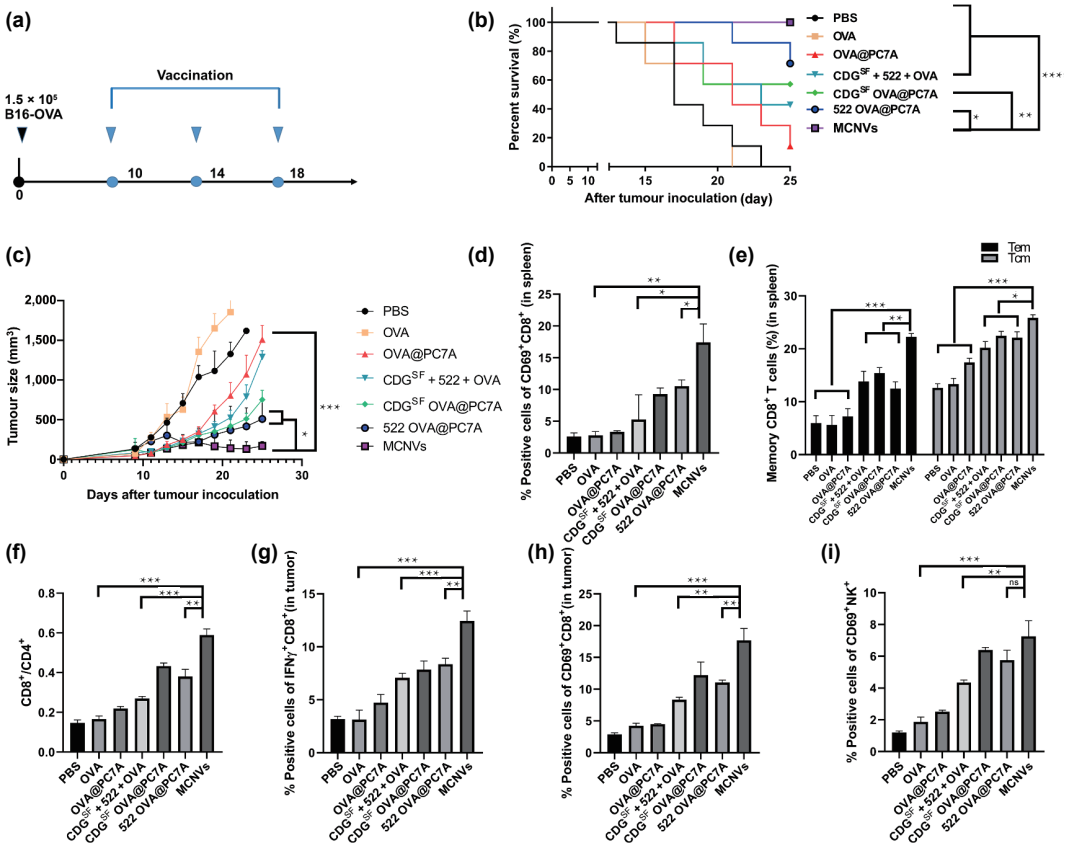

Figure 7 MCNV induces specific antitumor responses in a mouse model of melanoma. (a) Scheme of antitumor study. (b) Survival rate of B16-OVA tumor-bearing mice ($n = 7$). (c) Tumor growth curves in the B16-OVA melanoma model (mm^3) ($n = 7$). (d) Percentage of $CD69^+CD8^+$ T cells in splenocytes ($n = 4$). (e) Percentage of $CD44^+CD62L^-CD8^+$ Tem cells and $CD44^+CD62L^+CD8^+$ Tcm cells in splenocytes ($n = 4$). (f) Ratio of $CD8^+$ to $CD4^+$ T cells in the tumor microenvironment ($n = 4$). (g) Percentage of IFN-γ^+CD8^+ T cells in tumor (after *ex vivo* restimulation with OVA antigen) ($n = 4$). (h) and (i) Percentage of $CD69^+CD8^+$ T cells (h) and $CD69^+NK^+$ (i) in tumor after treatment in by each group ($n = 4$). The results are shown as the mean ± SD; ns: no significant difference, $^*p < 0.05$, $^{**}p < 0.01$, and $^{***}p < 0.001$ by Mantel-Cox test for survival rate (b), two-tailed Student's *t*-test for (c), and one-way ANOVA with Tukey's test for (d)–(i).

of MCNVs on the immune cell composition of B16-OVA melanoma TME. MCNV treatment increased the $CD8^+/CD4^+$ T cell ratio, which is a good prognostic indicator of the response to immunotherapy and clinical outcome [17, 18] (Fig. 7(f)). To verify the specificity of TILs, we stimulated TILs again with OVA for 4 h and performed flow cytometry analysis after staining the cells with IFN-γ antibody. The results showed that mice immunized with MCNVs induced the significant increase in the proportion of $CD8^+$ IFN-γ^+ T cells, exhibiting strong tumor specific immunity (Fig. 7(g)). These results were consistent with data from the spleen, and MCNVs markedly upregulated the levels of $CD69^+CD8^+$ T and NK cells in tumors compared with free adjuvant or single adjuvant nanoparticles (Figs. 7(h) and 7(i)), demonstrating that MCNVs effectively evoked lymphocytes in tumors.

4 Conclusions

In summary, we aimed to improve the immunogenicity of tumors as well as the proportion of tumor infiltrating lymphocytes. We selected the novel STING agonist CDG^{SF} as the immunostimulant in the vaccine system. However, CDG^{SF} alone can not elicit a broad and intense cytokine response; therefore, we added the TLR7/8 agonist 522 to address this issue. We used a combination of STING and TLR7/8 agonists for the first time in cancer immunotherapy. In addition, we identified synergistic immune effects of CDG^{SF} and 522, which possibly occurred through the NF-κB P65 and TBK-1 pathways. Subsequently, to further improve the cancer immunotherapy effect, we used PC7A NPs as carriers for adjuvants and introduced OVA as a model antigen to obtain MCNVs. The results showed that MCNVs were effective in activating DCs *in situ* after migrating to lymph nodes, which in turn triggered specific CTLs. After melanoma challenge, MCNVs-immunized mice exhibited increased tumor infiltrating IFN-γ^+CD8^+ T cells, resulting in a 100% survival rate in mice after 25 days. Because MCNVs elicit a robust immune response, they can be used as a platform for further applications in other types of diseases.

Acknowledgements

This work was supported by the National Key R&D Program of China (Nos. 2019YFA0904200 and 2018YFA0507600), Tsinghua University Spring Breeze Fund (No. 2020Z99CFY042), and the National Natural Science Foundation of China (No. 92053108).

Electronic Supplementary Material: Supplementary material (synthesis of CDG^{SF}, 522, PC7A and OVA; preparation of MCNVs; representative gating strategies for flow cytometry) is available in the online version of this article at https://doi.org/10.1007/s12274-022-4282-x.

References

[1] Mellman, I.; Coukos, G.; Dranoff, G. Cancer immunotherapy comes of age. *Nature* **2011**, *480*, 480–489.

[2] Sanmamed, M. F.; Chen, L. P. A paradigm shift in cancer immunotherapy: From enhancement to normalization. *Cell* **2018**, *175*, 313–326.

[3] Esfahani, K.; Roudaia, L.; Buhlaiga, N.; Del Rincon, S. V.; Papneja, N.; Miller, W. H. A review of cancer immunotherapy: From the past,

to the present, to the future. *Curr. Oncol.* **2020**, *27*, 87–97.
[4] Pardoll, D. M. The blockade of immune checkpoints in cancer immunotherapy. *Nat. Rev. Cancer* **2012**, *12*, 252–264.
[5] Ribas, A.; Wolchok, J. D. Cancer immunotherapy using checkpoint blockade. *Science* **2018**, *359*, 1350–1355.
[6] Hu, Z. T.; Ott, P. A.; Wu, C. J. Towards personalized, tumour-specific, therapeutic vaccines for cancer. *Nat. Rev. Immunol.* **2018**, *18*, 168–182.
[7] Liu, Y. F.; Sun, Z. Y.; Chen, P. G.; Huang, Z. H.; Gao, Y.; Shi, L.; Zhao, Y. F.; Chen, Y. X.; Li, Y. M. Glycopeptide nanoconjugates based on multilayer self-assembly as an antitumor vaccine. *Bioconjugate Chem.* **2015**, *26*, 1439–1442.
[8] Cai, H.; Huang, Z. H.; Shi, L.; Zou, P.; Zhao, Y. F.; Kunz, H.; Li, Y. M. Synthesis of Tn/T antigen MUC1 glycopeptide BSA conjugates and their evaluation as vaccines. *Eur. J. Org. Chem.* **2011**, *2011*, 3685–3689.
[9] Sun, Z. Y.; Chen, P. G.; Liu, Y. F.; Shi, L.; Zhang, B. D.; Wu, J. J.; Zhao, Y. F.; Chen, Y. X.; Li, Y. M. Self-assembled nano-immunostimulant for synergistic immune activation. *ChemBioChem* **2017**, *18*, 1721–1729.
[10] Irvine, D. J.; Hanson, M. C.; Rakhra, K.; Tokatlian, T. Synthetic nanoparticles for vaccines and immunotherapy. *Chem. Rev.* **2015**, *115*, 11109–11146.
[11] Shao, Y.; Sun, Z. Y.; Wang, Y. J.; Zhang, B. D.; Liu, D. S.; Li, Y. M. Designable immune therapeutical vaccine system based on DNA supramolecular hydrogels. *ACS Appl. Mater. Interfaces* **2018**, *10*, 9310–9314.
[12] Li, W. H.; Li, Y. M. Chemical strategies to boost cancer vaccines. *Chem. Rev.* **2020**, *120*, 11420–11478.
[13] Sun, Z. Y.; Chen, P. G.; Liu, Y. F.; Zhang, B. D.; Wu, J. J.; Chen, Y. X.; Zhao, Y. F.; Li, Y. M. Multi-component self-assembled anti-tumor nano-vaccines based on MUC1 glycopeptides. *Chem. Commun.* **2016**, *52*, 7572–7575.
[14] Beatty, G. L.; Gladney, W. L. Immune escape mechanisms as a guide for cancer immunotherapy. *Clin. Cancer Res.* **2015**, *21*, 687–692.
[15] Khalil, D. N.; Smith, E. L.; Brentjens, R. J.; Wolchok, J. D. Erratum: The future of cancer treatment: Immunomodulation, CARs and combination immunotherapy. *Nat. Rev. Clin. Oncol.* **2016**, *13*, 394.
[16] Gotwals, P.; Cameron, S.; Cipolletta, D.; Cremasco, V.; Crystal, A.; Hewes, B.; Mueller, B.; Quaratino, S.; Sabatos-Peyton, C.; Petruzzelli, L. et al. Prospects for combining targeted and conventional cancer therapy with immunotherapy. *Nat. Rev. Cancer* **2017**, *17*, 286–301.
[17] Fridman, W. H.; Zitvogel, L.; Sautès-Fridman, C.; Kroemer, G. The immune contexture in cancer prognosis and treatment. *Nat. Rev. Clin. Oncol.* **2017**, *14*, 717–734.
[18] Binnewies, M.; Roberts, E. W.; Kersten, K.; Chan, V.; Fearon, D. F.; Merad, M.; Coussens, L. M.; Gabrilovich, D. I.; Ostrand-Rosenberg, S.; Hedrick, C. C. et al. Understanding the tumor immune microenvironment (TIME) for effective therapy. *Nat. Med.* **2018**, *24*, 541–550.
[19] Mount, A.; Koernig, S.; Silva, A.; Drane, D.; Maraskovsky, E.; Morelli, A. B. Combination of adjuvants: The future of vaccine design. *Expert Rev. Vaccines* **2013**, *12*, 733–746.
[20] Deng, L. F.; Liang, H.; Xu, M.; Yang, X. M.; Burnette, B.; Arina, A.; Li, X. D.; Mauceri, H.; Beckett, M.; Darga, T. et al. STING-dependent cytosolic DNA sensing promotes radiation-induced type I interferon-dependent antitumor immunity in immunogenic tumors. *Immunity* **2014**, *41*, 843–852.
[21] Woo, S. R.; Fuertes, M. B.; Corrales, L.; Spranger, S.; Furdyna, M. J.; Leung, M. Y. K.; Duggan, R.; Wang, Y.; Barber, G. N.; Fitzgerald, K. A. et al. STING-dependent cytosolic DNA sensing mediates innate immune recognition of immunogenic tumors. *Immunity* **2014**, *41*, 830–842.
[22] Wu, J. J.; Zhao, L.; Hu, H. G.; Li, W. H.; Li, Y. M. Agonists and inhibitors of the STING pathway: Potential agents for immunotherapy. *Med. Res. Rev.* **2020**, *40*, 1117–1141.
[23] Jiang, M. L.; Chen, P. X.; Wang, L.; Li, W.; Chen, B.; Liu, Y.; Wang, H.; Zhao, S.; Ye, L. Y.; He, Y. Y. et al. cGAS-STING, an important pathway in cancer immunotherapy. *J. Hematol. Oncol.* **2020**, *13*, 81.
[24] Chen, Q.; Sun, L. J.; Chen, Z. J. Regulation and function of the cGAS-STING pathway of cytosolic DNA sensing. *Nat. Immunol.* **2016**, *17*, 1142–1149.
[25] Gao, P.; Ascano, M.; Zillinger, T.; Wang, W. Y.; Dai, P. H.; Serganov, A. A.; Gaffney, B. L.; Shuman, S.; Jones, R. A.; Deng, L. et al. Structure-function analysis of STING activation by c[G(2',5')pA(3',5')p] and targeting by antiviral DMXAA. *Cell* **2013**, *154*, 748–762.
[26] Corrales, L.; McWhirter, S. M.; Dubensky, T. W. Jr.; Gajewski, T. F. The host STING pathway at the interface of cancer and immunity. *J. Clin. Invest.* **2016**, *126*, 2404–2411.
[27] Li, A. P.; Yi, M.; Qin, S.; Song, Y. P.; Chu, Q.; Wu, K. M. Activating cGAS-STING pathway for the optimal effect of cancer immunotherapy. *J. Hematol. Oncol.* **2019**, *12*, 35.
[28] Fu, J.; Kanne, D. B.; Leong, M.; Glickman, L. H.; McWhirter, S. M.; Lemmens, E.; Mechette, K.; Leong, J. J.; Lauer, P.; Liu, W. Q. et al. STING agonist formulated cancer vaccines can cure established tumors resistant to PD-1 blockade. *Sci. Transl. Med.* **2015**, *7*, 283ra52.
[29] Demaria, O.; De Gassart, A.; Coso, S.; Gestermann, N.; Di Domizio, J.; Flatz, L.; Gaide, O.; Michielin, O.; Hwu, P.; Petrova, T. V. et al. STING activation of tumor endothelial cells initiates spontaneous and therapeutic antitumor immunity. *Proc. Natl. Acad. Sci. USA* **2015**, *112*, 15408–15413.
[30] Hanson, M. C.; Crespo, M. P.; Abraham, W.; Moynihan, K. D.; Szeto, G. L.; Chen, S. H.; Melo, M. B.; Mueller, S.; Irvine, D. J. Nanoparticulate STING agonists are potent lymph node-targeted vaccine adjuvants. *J. Clin. Invest.* **2015**, *125*, 2532–2546.
[31] Corrales, L.; Glickman, L. H.; McWhirter, S. M.; Kanne, D. B.; Sivick, K. E.; Katibah, G. E.; Woo, S. R.; Lemmens, E.; Banda, T.; Leong, J. J. et al. Direct activation of STING in the tumor microenvironment leads to potent and systemic tumor regression and immunity. *Cell Rep.* **2015**, *11*, 1018–1030.
[32] Nakamura, T.; Miyabe, H.; Hyodo, M.; Sato, Y.; Hayakawa, Y.; Harashima, H. Liposomes loaded with a STING pathway ligand, cyclic di-GMP, enhance cancer immunotherapy against metastatic melanoma. *J. Controlled Release* **2015**, *216*, 149–157.
[33] Curran, E.; Chen, X. F.; Corrales, L.; Kline, D. E.; Dubensky, T. W. Jr.; Duttagupta, P.; Kortylewski, M.; Kline, J. STING pathway activation stimulates potent immunity against acute myeloid leukemia. *Cell Rep.* **2016**, *15*, 2357–2366.
[34] Ohkuri, T.; Kosaka, A.; Ishibashi, K.; Kumai, T.; Hirata, Y.; Ohara, K.; Nagato, T.; Oikawa, K.; Aoki, N.; Harabuchi, Y. et al. Intratumoral administration of cGAMP transiently accumulates potent macrophages for anti-tumor immunity at a mouse tumor site. *Cancer Immunol. Immunother.* **2017**, *66*, 705–716.
[35] Koshy, S. T.; Cheung, A. S.; Gu, L.; Graveline, A. R.; Mooney, D. J. Liposomal delivery enhances immune activation by STING agonists for cancer immunotherapy. *Adv. Biosyst.* **2017**, *1*, 1600013.
[36] Gulen, M. F.; Koch, U.; Haag, S. M.; Schuler, F.; Apetoh, L.; Villunger, A.; Radtke, F.; Ablasser, A. Signalling strength determines proapoptotic functions of STING. *Nat. Commun.* **2017**, *8*, 427.
[37] Wu, J. J.; Li, W. H.; Chen, P. G.; Zhang, B. D.; Hu, H. G.; Li, Q. Q.; Zhao, L.; Chen, Y. X.; Zhao, Y. F.; Li, Y. M. Targeting STING with cyclic di-GMP greatly augmented immune responses of glycopeptide cancer vaccines. *Chem. Commun.* **2018**, *54*, 9655–9658.
[38] An, M.; Yu, C. S.; Xi, J. C.; Reyes, J.; Mao, G. Z.; Wei, W. Z.; Liu, H. P. Induction of necrotic cell death and activation of STING in the tumor microenvironment via cationic silica nanoparticles leading to enhanced antitumor immunity. *Nanoscale* **2018**, *10*, 9311–9319.
[39] Baird, J. R.; Bell, R. B.; Troesch, V.; Friedman, D.; Bambina, S.; Kramer, G.; Blair, T. C.; Medler, T.; Wu, Y. P.; Sun, Z. Y. et al. Evaluation of explant responses to STING ligands: Personalized immunosurgical therapy for head and neck squamous cell carcinoma. *Cancer Res.* **2018**, *78*, 6308–6319.
[40] Leach, D. G.; Dharmaraj, N.; Piotrowski, S. L.; Lopez-Silva, T. L.;

Lei, Y. L.; Sikora, A. G.; Young, S.; Hartgerink, J. D. STINGel: Controlled release of a cyclic dinucleotide for enhanced cancer immunotherapy. *Biomaterials* **2018**, *163*, 67–75.

[41] Park, C. G.; Hartl, C. A.; Schmid, D.; Carmona, E. M.; Kim, H. J.; Goldberg, M. S. Extended release of perioperative immunotherapy prevents tumor recurrence and eliminates metastases. *Sci. Transl. Med.* **2018**, *10*, eaar1916.

[42] Wilson, D. R.; Sen, R.; Sunshine, J. C.; Pardoll, D. M.; Green, J. J.; Kim, Y. J. Biodegradable STING agonist nanoparticles for enhanced cancer immunotherapy. *Nanomed. :Nanotechnol., Biol. Med.* **2018**, *14*, 237–246.

[43] Junkins, R. D.; Gallovic, M. D.; Johnson, B. M.; Collier, M. A.; Watkins-Schulz, R.; Cheng, N.; David, C. N.; McGee, C. E.; Sempowski, G. D.; Shterev, I. et al. A robust microparticle platform for a STING-targeted adjuvant that enhances both humoral and cellular immunity during vaccination. *J. Controlled Release* **2018**, *270*, 1–13.

[44] Collier, M. A.; Junkins, R. D.; Gallovic, M. D.; Johnson, B. M.; Johnson, M. M.; Macintyre, A. N.; Sempowski, G. D.; Bachelder, E. M.; Ting, J. P. Y.; Ainslie, K. M. Acetalated dextran microparticles for codelivery of STING and TLR7/8 agonists. *Mol. Pharmaceutics* **2018**, *15*, 4933–4946.

[45] Shae, D.; Becker, K. W.; Christov, P.; Yun, D. S.; Lytton-Jean, A. K. R.; Sevimli, S.; Ascano, M.; Kelley, M.; Johnson, D. B.; Balko, J. M. et al. Endosomolytic polymersomes increase the activity of cyclic dinucleotide STING agonists to enhance cancer immunotherapy. *Nat. Nanotechnol.* **2019**, *14*, 269–278.

[46] Hu, H. G.; Wu, J. J.; Zhang, B. D.; Li, W. H.; Li, Y. M. Pam_3CSK_4-CDG^{SF} augments antitumor immunotherapy by synergistically activating TLR1/2 and STING. *Bioconjugate Chem.* **2020**, *31*, 2499–2503.

[47] Li, S. X.; Luo, M.; Wang, Z. H.; Feng, Q.; Wilhelm, J.; Wang, X.; Li, W.; Wang, J.; Cholka, A.; Fu, Y. X. et al. Prolonged activation of innate immune pathways by a polyvalent STING agonist. *Nat. Biomed. Eng.* **2021**, *5*, 455–466.

[48] Wu, J. J.; Zhao, L.; Han, B. B.; Hu, H. G.; Zhang, B. D.; Li, W. H.; Chen, Y. X.; Li, Y. M. A novel STING agonist for cancer immunotherapy and a SARS-CoV-2 vaccine adjuvant. *Chem. Commun.* **2021**, *57*, 504–507.

[49] Staats, H. F.; Ennis, F. A. Jr. IL-1 is an effective adjuvant for mucosal and systemic immune responses when coadministered with protein immunogens. *J. Immunol.* **1999**, *162*, 6141–6147.

[50] Huang, T.; Zhao, K. L.; Zhang, Z. Q.; Tang, C.; Zhang, X. Y.; Yue, B. S. DNA vaccination based on pyolysin co-immunized with IL-1β enhances host antibacterial immunity against *Trueperella pyogenes* infection. *Vaccine* **2016**, *34*, 3469–3477.

[51] Metzger, D. W. Interleukin-12 as an adjuvant for induction of protective antibody responses. *Cytokine* **2010**, *52*, 102–107.

[52] Stevceva, L.; Moniuszko, M.; Ferrari, M. G. Utilizing IL-12, IL-15 and IL-7 as mucosal vaccine adjuvants. *Lett. Drug Des. Discov.* **2006**, *3*, 586–592.

[53] Diehl, S. A.; Schmidlin, H.; Nagasawa, M.; Blom, B.; Spits, H. IL-6 triggers IL-21 production by human $CD4^+$ T cells to drive STAT3-dependent plasma cell differentiation in B cells. *Immunol. Cell Biol.* **2012**, *90*, 802–811.

[54] Arulanandam, B. P.; O'Toole, M.; Metzger, D. W. Intranasal interleukin-12 is a powerful adjuvant for protective mucosal immunity. *J. Infect. Dis.* **1999**, *180*, 940–949.

[55] Arulanandam, B. P.; Mittler, J. N.; Lee, W. T.; O'Toole, M.; Metzger, D. W. Neonatal administration of IL-12 enhances the protective efficacy of antiviral vaccines. *J. Immunol.* **2000**, *164*, 3698–3704.

[56] Ichinohe, T.; Lee, H. K.; Ogura, Y.; Flavell, R.; Iwasaki, A. Inflammasome recognition of influenza virus is essential for adaptive immune responses. *J. Exp. Med.* **2009**, *206*, 79–87.

[57] Kayamuro, H.; Yoshioka, Y.; Abe, Y.; Arita, S.; Katayama, K.; Nomura, T.; Yoshikawa, T.; Kubota-Koketsu, R.; Ikuta, K.; Okamoto, S. et al. Interleukin-1 family cytokines as mucosal vaccine adjuvants for induction of protective immunity against influenza virus. *J. Virol.* **2010**, *84*, 12703–12712.

[58] Schulz, E. G.; Mariani, L.; Radbruch, A.; Höfer, T. Sequential polarization and imprinting of type 1 T helper lymphocytes by interferon-γ and interleukin-12. *Immunity* **2009**, *30*, 673–683.

[59] Randolph, G. J.; Angeli, V.; Swartz, M. A. Dendritic-cell trafficking to lymph nodes through lymphatic vessels. *Nat. Rev. Immunol.* **2005**, *5*, 617–628.

[60] Bousso, P. T-cell activation by dendritic cells in the lymph node: Lessons from the movies. *Nat. Rev. Immunol.* **2008**, *8*, 675–684.

[61] Smith, D. M.; Simon, J. K.; Baker, J. R. Jr. Applications of nanotechnology for immunology. *Nat. Rev. Immunol.* **2013**, *13*, 592–605.

[62] Trevaskis, N. L.; Kaminskas, L. M.; Porter, C. J. H. From sewer to saviour—Targeting the lymphatic system to promote drug exposure and activity. *Nat. Rev. Drug Discov.* **2015**, *14*, 781–803.

[63] Goldberg, M. S. Improving cancer immunotherapy through nanotechnology. *Nat. Rev. Cancer* **2019**, *19*, 587–602.

[64] Zhou, K. J.; Wang, Y. G.; Huang, X. N.; Luby-Phelps, K.; Sumer, B. D.; Gao, J. M. Tunable, ultrasensitive pH-responsive nanoparticles targeting specific endocytic organelles in living cells. *Angew. Chem., Int. Ed.* **2011**, *50*, 6109–6114.

[65] Luo, M.; Wang, H.; Wang, Z. H.; Cai, H. C.; Lu, Z. G.; Li, Y.; Du, M. J.; Huang, G.; Wang, C. S.; Chen, X. et al. A STING-activating nanovaccine for cancer immunotherapy. *Nat. Nanotechnol.* **2017**, *12*, 648–654.

[66] Aroh, C.; Wang, Z. H.; Dobbs, N.; Luo, M.; Chen, Z. J.; Gao, J. M.; Yan, N. Innate immune activation by cGMP-AMP nanoparticles leads to potent and long-acting antiretroviral response against HIV-1. *J. Immunol.* **2017**, *199*, 3840–3848.

[67] Luo, M.; Liu, Z. D.; Zhang, X. Y.; Han, C. H.; Samandi, L. Z.; Dong, C. B.; Sumer, B. D.; Lea, J.; Fu, Y. X.; Gao, J. M. Synergistic STING activation by PC7A nanovaccine and ionizing radiation improves cancer immunotherapy. *J. Controlled Release* **2019**, *300*, 154–160.

[68] Feng, Q.; Wilhelm, J.; Gao, J. M. Transistor-like ultra-pH-sensitive polymeric nanoparticles. *Acc. Chem. Res.* **2019**, *52*, 1485–1495.

[69] Wilhelm, J.; Wang, Z. H.; Sumer, B. D.; Gao, J. M. Exploiting nanoscale cooperativity for precision medicine. *Adv. Drug Deliv. Rev.* **2020**, *158*, 63–72.

[70] Li, S. X.; Bennett, Z. T.; Sumer, B. D.; Gao, J. M. Nano-immune-engineering approaches to advance cancer immunotherapy: Lessons from ultra-pH-sensitive nanoparticles. *Acc. Chem. Res.* **2020**, *53*, 2546–2557.

[71] Wilhelm, J.; Quinoñes-Pérez, M.; Wang, J.; Wang, X.; Basava, V. S.; Gao, J. M. Antigen folding improves loading efficiency and antitumor efficacy of PC7A nanoparticle vaccine. *J. Controlled Release* **2021**, *329*, 353–360.

[72] Kim, H.; Niu, L.; Larson, P.; Kucaba, T. A.; Murphy, K. A.; James, B. R.; Ferguson, D. M.; Griffith, T. S.; Panyam, J. Polymeric nanoparticles encapsulating novel TLR7/8 agonists as immunostimulatory adjuvants for enhanced cancer immunotherapy. *Biomaterials.* **2018**, *164*, 38–53.

[73] Schiaffo, C. E.; Shi, C.; Xiong, Z. M.; Olin, M.; Ohlfest, J. R.; Aldrich, C. C.; Ferguson, D. M. Structure-activity relationship analysis of imidazoquinolines with Toll-like receptors 7 and 8 selectivity and enhanced cytokine induction. *J. Med. Chem.* **2014**, *57*, 339–347.

[74] Schmitz, N.; Kurrer, M.; Bachmann, M. F.; Kopf, M. Interleukin-1 is responsible for acute lung immunopathology but increases survival of respiratory influenza virus infection. *J. Virol.* **2005**, *79*, 6441–6448.

[75] Guglani, L.; Khader, S. A. Th17 cytokines in mucosal immunity and inflammation. *Curr. Opin. HIV AIDS* **2010**, *5*, 120–127.

[76] Warger, T.; Osterloh, P.; Rechtsteiner, G.; Fassbender, M.; Heib, V.; Schmid, B.; Schmitt, E.; Schild, H.; Radsak, M. P. Synergistic activation of dendritic cells by combined Toll-like receptor ligation induces superior CTL responses *in vivo*. *Blood.* **2006**, *108*, 544–550.

[77] Trinchieri, G.; Sher, A. Cooperation of Toll-like receptor signals in innate immune defence. *Nat. Rev. Immunol.* **2007**, *7*, 179–190.

[78] Hu, Y.; Cong, X. Y.; Chen, L.; Qi, J.; Wu, X. J.; Zhou, M. M.; Yoo, D.; Li, F.; Sun, W. B.; Wu, J. Q. et al. Synergy of TLR3 and 7 ligands significantly enhances function of DCs to present inactivated PRRSV antigen through TRIF/MyD88-NF-κB signaling pathway. *Sci. Rep.* **2016**, *6*, 23977.

[79] Bocanegra Gondan, A. I.; Ruiz-de-Angulo, A.; Zabaleta, A.; Gómez Blanco, N.; Cobaleda-Siles, B. M.; García-Granda, M. J.; Padro, D.; Llop, J.; Arnaiz, B.; Gato, M. et al. Effective cancer immunotherapy in mice by polyIC-imiquimod complexes and engineered magnetic nanoparticles. *Biomaterials* **2018**, *170*, 95–115.

[80] Matsumoto, M.; Seya, T. TLR3: Interferon induction by double-stranded RNA including poly(I:C). *Adv. Drug Deliv. Rev.* **2008**, *60*, 805–812.

[81] Krieg, A. M. Therapeutic potential of Toll-like receptor 9 activation. *Nat. Rev. Drug Discov.* **2006**, *5*, 471–484.

[82] Dellacherie, M. O.; Seo, B. R.; Mooney, D. J. Macroscale biomaterials strategies for local immunomodulation. *Nat. Rev. Mater.* **2019**, *4*, 379–397.

[83] Milling, L.; Zhang, Y.; Irvine, D. J. Delivering safer immunotherapies for cancer. *Adv. Drug Deliv. Rev.* **2017**, *114*, 79–101.